Carbohydrate Polymers 84 (2011) 364–372

Contents lists available at ScienceDirect

Carbohydrate Polymers

journal homepage: www.elsevier.com/locate/carbpol

Characterization of chitosan magnetic nanoparticles for in situ delivery of tissue plasminogen activator

Jyh-Ping Chen[a,*], Pei-Chin Yang[a], Yunn-Hwa Ma[b], Tony Wu[c]

[a] Department of Chemical and Materials Engineering, Chang Gung University, 259 Wen Hwa 1st Rd., Kwei-San, Taoyuan 333, Taiwan, ROC
[b] Department of Physiology and Pharmacology, Chang Gung University, Kwei-San, Taoyuan 333, Taiwan, ROC
[c] Department of Neurology, Chang Gung Memorial Hospital, Kwei-San, Taoyuan 333, Taiwan, ROC

ARTICLE INFO

Article history:
Received 29 September 2010
Received in revised form
19 November 2010
Accepted 19 November 2010
Available online 26 November 2010

Keywords:
Magnetic nanoparticles
Chitosan
Drug delivery
Thrombolysis
Tissue plasminogen activator

ABSTRACT

In this study, we examine the preparation of chitosan-coated magnetic nanoparticle (MNP) (chitosan-MNP) and the feasibility of using tissue plasminogen activator (tPA) covalently bound to chitosan-MNP surface (chitosan-MNP–tPA) for magnetic targeted delivery of the thrombolytic drug. The physicochemical properties of chitosan-MNP prepared with increasing chitosan/MNP ratios were characterized in detail. The optimum drug loading is reached when 0.5 mg tPA is conjugated with 5 mg chitosan-MNP where 95% drug is attached to the carrier with full retention of its thrombolytic activity. Under magnetic guidance, chitosan-MNP–tPA can reduce the blood clot lysis time by 58% compared with runs without magnetic targeting or by 53% compared with free tPA using the same drug dosage. Effective thrombolysis in response to chitosan-MNP–tPA under magnetic guidance is also demonstrated in a rat embolic model where one-fifth of the dose of tPA may exert similar thrombolytic efficacy of the drug.

1. Introduction

Tissue plasminogen activator (tPA) is one of the thrombolytic drugs widely used in the treatment of established thrombus in myocardial infarction and pulmonary embolism (Smith, 1999). With the use of thrombolytic drugs, early mortality from acute myocardial infarction has been reduced by approximately one-third (Anderson & Willerson, 1993). However, the exceedingly short half-lives (<5 min) of tPA require its administration in large doses (1 mg/kg) to yield positive effects, although the effective therapeutic dose range of tPA at the thrombus site is only around 0.45–1.00 mg/ml (Huber, Runge, Bode, & Gulba, 1996). As a consequence, this inevitably leads to a significant incidence of hemorrhagic complications. Although several approaches have been attempted, current thrombolytic therapy is still hampered by a high incidence of bleeding complications. A drug delivery approach to deliver tPA under magnetic guidance for targeted thrombolysis will allow tPA to act only at the site of the target. This would potentially reduce the total administered dose of the drug necessary for the treatment, and hence its hemorrhagic side effects (Kaminski et al., 2008; Ma et al., 2009; Xie et al., 2007).

Magnetic nanoparticles (MNPs) offer several advantages when used as a drug carrier, including the large surface area, which can be properly modified to attach with drug molecules. Ensuring biocompatibility and non-toxicity, iron oxide based particles (magnetite) with superparamagnetic characteristics are commonly used as the magnetically responsive component, which can be manipulated by an external magnetic field gradient. The superparamagnetic behavior implies that its magnetization disappears once the external magnetic field is removed. Based on these properties, the superparamagnetic nanoparticles could be transported through the vascular system, concentrated in a specific part of the body with the aid of a magnetic field, and used as a carrier for tPA delivery. Target delivery of tPA covalently bound to MNP will ensure the thrombolytic drug to be delivered under magnetic guidance and retained in a local area in circulation (Wu et al., 2007), which is potentially useful for targeting fibrin clot in vivo.

For drug delivery applications, iron oxide MNP must be precoated with substances that assure their stability, biodegradability, and non-toxicity in the physiological medium in order to achieve combined properties of high magnetic saturation, biocompatibility and interactive functions on the surface (Gupta & Gupta, 2005). The surfaces of these particles could be modified through a coating process by depositing a few atomic layers of biocompatible polymers. The polymer coating not only leads to the creation of more hydrophilic nanostructures but also provides a variety of surface functional groups to bind drug molecules, inhibit aggregation, and

* Corresponding author. Tel.: +886 3 2118800; fax: +886 3 2118668.
E-mail addresses: jpchen@mail.cgu.edu.tw, jpchen1125@hotmail.com (J.-P. Chen).

0144-8617/$ – see front matter © 2010 Elsevier Ltd. All rights reserved.
doi:10.1016/j.carbpol.2010.11.052

increase stability (Dobson, 2006; Fang & Zhang, 2009). Both natural and synthetic polymers have been used in the preparation of coated MNP (Tartaj, Morales, Gonzalez-Carreno, Veintemillas-Verdaguer, & Serna, 2005).

Magnetic nanoparticles are physiologically inert, but upon intravenous injection the surface of MNP is subjected to adsorption by plasma proteins, or opsonization, as the first step in their clearance by the reticuloendothelial system (Berry & Curtis, 2003). Surface modification of MNP by coating with a layer of hydrophilic polysaccharide diminishes coating by plasma components and allows MNP to remain in the blood stream for a longer period of time (Gaur et al., 2000). Chitosan is a polysaccharide produced by deacetylation of chitin naturally extracted from shells of crabs and shrimps, or isolated from the cell walls of fungi. Chitosan is a unique cationic, hydrophilic polymer that has beneficial properties, such as low toxicity, low immunogenicity, excellent biodegradability, biocompatibility as well as a high positive charge that easily forms polyelectrolyte complexes with negatively charged entities (Majeti & Kumar, 2000). It is being investigated in the pharmaceutical industry for its potential in the development of drug delivery systems (Denkbas & Ottenbrite, 2006). Chitosan interacts with negatively charged DNA and protects it from nuclease degradation, which makes it a good candidate for nonviral gene delivery (Dang & Leong, 2006). Chitosan nanoparticles have been used effectively to transfect cells with siRNA (Katas & Alpar, 2006) and siRNA delivered using chitosan nanoparticles resulting in efficient gene silencing in ovarian carcinoma (Sood et al., 2009).

Although chitosan and its derivatives have been used to form polymeric nanoparticles through electrostatic complexation with nucleic acids and various pharmaceutical formulations (Janes, Calvo, & Alonso, 2001), only recently has chitosan been used in combination with iron oxide MNP (Donadel et al., 2008; Huang, Shieh, Shih, & Twu, 2010; Li, Jiang, Huang, Ding, & Chen, 2008). To coat iron oxide MNP with chitosan, it has been found that direct, in situ coating is problematic because of its poor solubility at pH values necessary to precipitate MNP (Kumar, Muzzarelli, Muzzarelli, Sashiwa, & Domb, 2004). Chitosan-coated MNP has been produced, though, by physically adsorbing chitosan onto oleic acid-coated nanoparticles yielding spherically shaped chitosan-MNP with 15 nm diameter (Kim, Lee, Kwak, & Kim, 2005).

In a recent study, tPA encapsulated in chitosan-coated poly-(lactide-co-glycolide) nanoparticles was used for accelerating thrombolysis (Chung, Wang, & Tsai, 2008). Although chitosan has been reported to be an effective hemostasis material, chitosan-coated nanoparticles were not found to cause blood clot by contacting with whole blood in the study. Nanoparticles coated with chitosan can significantly shorter clot lysis times and have higher weight percentages of digested clots than uncoated nanoparticles, suggesting a beneficial effect of chitosan on blood clots lysis. This was explained by the positive surface zeta potential of chitosan-coated nanoparticles, which facilitates the penetration of the nanoparticles into blood clots containing the negatively charged fibrin at the physiological pH. Therefore, chitosan-coated MNP seems promising for magnetic targeted delivery of tPA. In this study, we immobilized tPA to chitosan-MNP by covalent binding and determine the enzyme activity and thrombolysis ability of the enzyme conjugate.

2. Materials and methods

2.1. Materials

Recombinant tissue plasminogen activator (tPA, Actilyse®) was obtained from Boehringer Ingelheim (Mannheim, Germany). Fe(II) chloride tetrahydate (99%), Fe (III) chloride hexahydrate (97%) were obtained from Acros. Chitosan polymer (150 kDa) with a degree of deacetylation of 95% was obtained from Fluka. Aqueous acetic acid (Aldrich) solution was used as a solvent for the chitosan and glutaraldehyde (Merck) was used as the cross-linking agent. [3-(4,5-Dimethylthiazol-2-yl)-2,5-diphenyl-tetrazolium bromide] (MTT), thrombin, and fibrinogen were obtained from Sigma. The chromogenic substrate, H-D-Isoleucyl-L-prolyl-L-arginine-pnitroaniline (S-2288) was obtained from Chromogenix. All the chemicals were of reagent grade and used without further purification.

2.2. Synthesis of Fe_3O_4 magnetic nanoparticle and chitosan-coated magnetic nanoparticle

Iron oxide MNP was obtained by reacting 2.375 g of $FeCl_3{\cdot}6H_2O$, and 0.875 g of $FeCl_2{\cdot}4H_2O$ in 40 ml of distilled deionized water at 60 °C under N_2 by stirring at 400 rpm for 1 h. One hundred milliliters of 8 M NH_4OH was added to the solution, after which the color of the mixture turned from yellow to black immediately, and the solution was stirred at 400 rpm for another 30 min. The synthesized Fe_3O_4 MNP was washed three times with 5% NH_4OH by magnetic decantation. Chitosan solution was prepared by dissolving the required amount of chitosan powder in 2% acetic acid solution. Ten milliliters of Fe_3O_4 MNP suspension (50 mg/ml) was poured into 40 ml of chitosan solution with vigorous stirring. Chitosan-MNP was prepared by reacting 0.5 g MNP with 0.0625, 0.125, 0.25, 0.5, or 1 g chitosan (the sample is called C125, C250, C500, C1000, or C2000). The solutions were then mixed via ultrasonication (20 kHz, 600 W) for 40 min. After the reaction, the chitosan-coated MNP was washed with 250 ml of 0.1 M phosphate buffer (pH 6) in 5 aliquots, and dispersed in the same buffer solution by ultrasonication for 30 s to reach a concentration of 10 mg/ml for storage at 4 °C.

2.3. Characterization of synthesized magnetic nanoparticles

A transmission electron microscope (TEM, JEOL JEM-2000 EX II) was used to observe morphology and particle size of nanoparticles. An aqueous dispersion of the particles was drop-cast onto a carbon-coated copper grid, and the grid was air-dried at room temperature before loading into the microscope. Alternative, the sample was stained with 2% phosphotungstic acid aqueous solution for 3 min before analysis. An atomic force microscope (Parks XE-100) was used to analyze surface topography and size of nanoparticles. Diluted nanoparticles in alcohol were deposited onto a freshly cleaved mica substrate and imaged after alcohol evaporation. Experiments were performed with a tapping mode and all images were recorded in air at room temperature in 256 pixels, with a scan size of 0.5 μm × 0.5 μm and a scan speed of 0.9 Hz.

The crystal structures of the nanoparticles were determined by wide angle X-ray diffraction (XRD, Siemens D5005 diffractometer) using a CuK_α source, a quartz monochrometer, and a geniometric plate at a scanning speed of 2° min^{-1} from 20° to 70°. The phases were identified by comparison with the JCPDS database. The zeta potential and the hydrodynamic particle diameter of nanoparticles were determined by laser dynamic light scattering with Malvern Zetasizer ZA 90 in water at 25 °C. The samples (20 μl) were diluted with 1 ml of DDI water and sonicated before measurements.

The magnetization of nanoparticles was measured by a superconducting quantum interference device magnetometer (Quantum Design MPMS XL-7) at 25 °C and ±10,000 G applied magnetic field. For Fourier transform infrared spectroscopy (FTIR) measurement using a Horiba FT-730 spectrometer, the samples were blended with KBr and then compressed to form a pellet. The transmission spectra were obtained from 600 to 4000 cm^{-1} with a resolution of 4 cm^{-1} and the number of scans was 128. The chitosan content

of chitosan-MNP was determined by thermogravimetric and differential thermal analysis (STA 449 PC, Netzsch). Analyses were performed with 20 mg of samples in a platinum pan under nitrogen atmosphere. The nominal gas flow was 5 ml/min, and the heating velocity was 10 °C/min. Concentrations of amino groups on the surface of chitosan-MNP were determined by the o-phthaldialdehyde method, which is based on the reaction of primary amines with an excess of o-phthaldialdehyde and β-mercaptoethanol and subsequent quantitative determination of unreacted o-phthaldialdehyde by reaction with glycine (Janolino & Swaisgood, 1992). The iron contents of chitosan-MNP were analyzed by inductively coupled plasma optical emission spectroscopy (Perkin Elmer Optima 2100 DV).

For in vitro biocompatibility test, the cytotoxic effects of chitosan-MNP were tested on a mouse embryonic fibroblast cell line (3T3). The 3T3 cells were cultured using 24-well culture plates (2.2×10^5 cells/well) in DMEM medium supplemented with 10% fetal bovine serum and incubated at 37 °C in a 5% CO_2 atmosphere. After 24 h of culture, the medium in the wells was replaced with fresh medium containing nanoparticles at a concentration ranging from 10^{-5} to 10^5 nM and cultured for another 24 h before measuring mitochondria activity by MTT assay. Fifty microliters of MTT dye solution (5 mg/ml in 0.1 M phosphate buffer, pH 7.4) was added to each well. After 4 h incubation at 37 °C in 5% CO_2, the medium was removed and the formazan crystals were dissolved in 0.05 ml of dimethylsulfoxide, and the solution was mixed vigorously to dissolve the crystal product. The optical density (OD) of each well was recorded on a microplate reader (BioTek Synergy HT) at 540 nm. The relative cell viability (%) related to the control well containing the cell culture medium without nanoparticles suspension was calculated using the following formula: $(OD_{sample}/OD_{control}) \times 100\%$.

2.4. Immobilization of tissue plasminogen activator

Five hundred microliters of chitosan-MNP suspension (10 mg/ml) was mixed with 0.1 ml of 0.5% glutaraldehyde for 30 min with shaking (160 rpm) and followed by washing twice with 2 ml phosphate buffer solution (0.1 M, pH 6.0). Two hundred and fifty microliters of activated chitosan-MNP (20 mg/ml) was then mixed with 0.25 ml of tPA solution (2 mg/ml) for 12 h at 4 °C under stirring at 50 rpm. Chitosan-MNP–tPA could be obtained after magnetic separation from the solution and washing with phosphate buffered saline (PBS, 137 mM NaCl, 2.7 mM KCl, 10 mM sodium phosphate dibasic, 2 mM potassium phosphate monobasic, pH 7.4). The amount of tPA immobilized to chitosan-MNP was determined by measuring unbound tPA protein concentrations in the supernatant and washing solution by a colorimetric method at 595 nm with the Protein Assay Kit from Bio-Rad. Protein loading efficiency was defined as the percentage of the weight of tPA protein bound to chitosan-MNP compared to that added during the immobilization step.

2.5. Activity assays of tissue plasminogen activator

Amidolytic activity of tPA was measured spectrophotometrically using the protease substrate S-2288™, a specific chromogenic substrate for tPA, according to manufacturer's instruction. Activity retention after immobilization was defined as the percentage of specific activity (U/mg) of immobilized tPA compared to that of free tPA, which is 2.35 U/mg.

Fibrinolytic activity of tPA was determined from fibrin clot lysis assay using fibrin-containing agarose plates (Liang, Song, Li, & Yang, 2000). The plates were prepared by mixing 5.0 ml low melting-temperature agarose solution (3.0%) containing 2.5 U thrombin with 5.0 ml fibrinogen solution (5 mg/ml) at 50 °C. The reaction mixture was poured into a 9 cm culture dish and cooled at 4 °C for 30 min until the fibrin clot became visible. To perform the assays, 0.1 ml of tPA solution or chitosan-MNP–tPA suspension was added into the round sample wells (3 mm diameter) made on the solidified fibrin–agarose gel and incubated at 37 °C overnight. The degree of fibrin lysis was quantified by comparing the size of the fibrin lysis zone around sample wells containing equivalent tPA concentrations.

2.6. Ex vivo thrombolysis model and in vivo rat embolic model

An ex vivo intravascular thrombolysis model driven by a constant pressure gradient, which is similar to the condition that maintains blood circulation in vivo, was used to determine blood clot lysis induced by tPA or chitosan-MNP–tPA (Berny et al., 2010) (Fig. 1). A 0.02 mm × 0.2 mm × 50 mm glass capillary tube (Vitrotube, VitroCom) was coated with collagen (100 μg/ml) for 1 h at room temperature and blocked with bovine serum albumin (5 mg/ml) for 1 h. The capillary was vertically mounted below a reservoir (ID = 0.75 cm) and immersed in a PBS bath. The length of capillary above and below the liquid height in the PBS bath is h_c (4.2 cm) and h_p (0.7 cm), respectively. Whole blood samples (0.5 ml) were mixed with 0.1 ml of 0.9% NaCl and 0.15% $CaCl_2$ solution containing 50 U thrombin to produce a blood clot (thickness h_b = 1 cm) at the bottom of the reservoir. Tissue plasminogen activator (0.1 mg/ml) in PBS, 10 mg/ml chitosan-MNP–tPA (prepared with C250) in PBS equivalent to 0.1 mg/ml tPA, or 10 mg/ml chitosan-MNP (C250) in PBS was introduced above the blood clot to a height of 1.2 cm (h_s) in the reservoir. For magnetic targeting, a magnet (6000 G) was placed close to and slowly circled around the reservoir at 6 rpm. After thrombolysis by tPA, blood was allowed to drain from the reservoir, through the capillary, into the PBS bath. Time to blood flow (blood clot lysis time) was recorded as the time when blood first exited from the capillary into the PBS bath. Experiments were observed over a 300 min period. If blood flow did not occur after 300 min, experiments were terminated.

An in vivo rat embolic model experiment was performed as described previously (Ma et al., 2007, 2009). The protocol was approved by the Institutional Animal Care and Use Committee of Chang Gung University. Briefly, the right iliac artery of anesthetized Sprague–Dawley rats was cannulated with a catheter for injection of blood clot and chitosan-MNP–tPA. Tissue perfusion of the left hind limb was measured with laser Doppler flowmetry (MoorFLPI, Moor Instruments). After equilibration, a piece of whole blood clot was injected via the right iliac artery and lodged in the left iliac artery. After 5 min, chitosan-MNP–tPA with a volume less than 150 μl was injected within 5 min and guided under an NdFeB magnet (4.9 kG) back and forth between the bifurcation and the femoral artery at a frequency of 6–10 rpm. Tissue perfusion was recorded for 2 h after injection of the clot.

2.7. Statistical analysis

Values are expressed as mean ± SE and are examined by one-way analysis of variance (ANOVA) and Tukey's test. Statistical significance was declared when a p value < 0.05.

3. Results and discussion

3.1. Preparation and properties of chitosan-coated magnetic nanoparticles

Iron oxide MNP was prepared by the chemical co-precipitation of ferric and ferrous salts in alkaline medium. To prevent aggregation of MNP, chitosan was used as a dispersing agent and coated to MNP surface. From the TEM micrograph in Fig. 2a, the electronic dense part (magnetite) of chitosan-MNP shows uniform

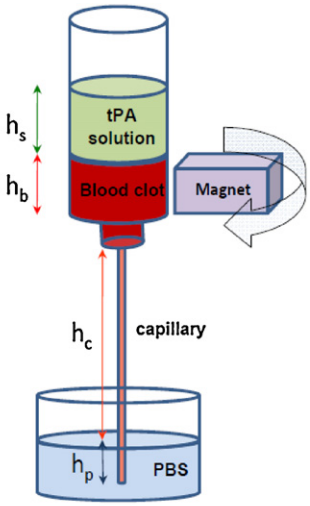

Treatment	Time to blood flow from capillary (min)
PBS	> 300
tPA	161.0 ± 8.5*
Chitosan-MNP-tPA (magnet)	76.3 ± 7.5
Chitosan-MNP-tPA (no magnet)	181.5 ± 7.8*
Chitosan-MNP (magnet)	> 300
Chitosan-MNP (no magnet)	> 300

*p <0.05 compared with chitosan-MNP-tPA (magnet), $n = 5$

Fig. 1. An ex vivo thrombolysis model for determining the magnetic targeting of blood clot by tPA immobilized to chitosan-coated magnetic nanoparticles (chitosan-MNP–tPA).

particle morphology. The average diameter was estimated for each preparation and the values were from 8.1 to 9.0 nm (Table 1). The diameters of these particles indicated that the synthesized MNP is superparamagnetic (Sun, Lee, & Zhang, 2008). Selected area electron diffraction patterns from Fig. 2a are shown in the insert, which confirms the nanoparticles were Fe_3O_4 and well crystallized. The core-shell structure of chitosan-coated magnetic nanoparticles was revealed with 2% phosphotungstic acid staining. Nanoparticles with slightly deformed round contours and diameters around 110 nm were observed, due to the selective staining of chitosan (Fig. 2b). Multiple Fe_3O_4 MNPs were entrapped and dispersed inside chitosan-MNP, whose boundary was lined with a chitosan layer of ~10 nm thickness. The morphology and particles size of magnetite within chitosan-MNP were also determined by atomic force microscope (Fig. 2c), which illustrated topographic images of clustered magnetite of the same size as observed from TEM in Fig. 2a.

Dynamic light scattering measurements of the particles showed the hydrodynamic diameters of chitosan-MNP were about 139–179 nm (Table 1). It should be noted the measured hydrodynamic diameter is for the whole chitosan-MNP but not for the opaque crystallites detected by TEM in Fig. 2a or that calculated from XRD, which is the particle size of individual Fe_3O_4 MNP. Multiple associations of Fe_3O_4 MNPs with chitosan polymer chains resulted in aggregates and increased the hydrodynamic diameter of chitosan-MNP, which can be compared with the value obtained from TEM after phosphotungstic acid staining (Fig 2b). The particle size from light scattering is larger than that from TEM due to par-

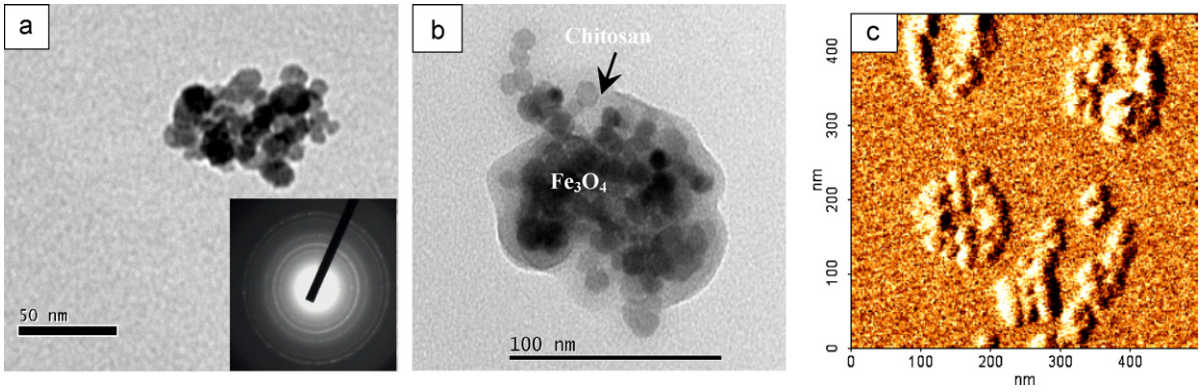

Fig. 2. Transmission electron microscope images of chitosan-coated magnetic nanoparticles (C250) before (a), and after (b) staining with phosphotungstic acid. (c) Atomic force microscope image of chitosan-MNP (C250). Insert in (a) is electron diffraction pattern.

Table 1
Properties of chitosan-coated magnetic nanoparticles (C125–C1000).

Sample[a]	MNP diameter (nm)		Hydrodynamic diameter[b] (nm)	Zeta potential (mV)	$-NH_2$[c] (μmole/mg)	Chitosan content[d] (%(w/w))	Fe_3O_4 Content[e] (%(w/w))
	TEM	XRD					
C125	8.1 ± 0.1	9.3	139.2	+20.3	119.5 ± 1.4	1.43	99.8 ± 2.8
C250	8.4 ± 0.1	9.5	152.5	+22.6	294.5 ± 1.2	2.37	97.3 ± 3.1
C500	8.7 ± 0.3	9.3	159.4	+27.3	590.0 ± 1.4	8.12	90.5 ± 5.5
C1000	8.7 ± 0.2	9.5	179.0	+28.4	1700 ± 1.0	30.01	70.2 ± 2.6
C2000	9.0 ± 0.2	9.6	155.4	+33.2	1962 ± 2.7	57.38	40.7 ± 5.2
MNP	8.5 ± 0.4	10.0	263.6	−28.4	–	–	–

[a] C125 is 1 g Fe_3O_4 magnetic nanoparticle (MNP) coated with 0.125 g chitosan. MNP is Fe_3O_4 MNP without chitosan coating.
[b] From dynamic light scattering.
[c] By the o-phthaldialdehyde method.
[d] From thermogravimetric and differential thermal analysis calculations.
[e] From inductively coupled plasma optical emission spectroscopy measurements.

ticle shrinkage after the drying process when preparing the TEM sample.

Electrophoretic mobility measurements gave a highly positive zeta potential after chitosan coating where the zeta potential increased from −28.4 mV for Fe_3O_4 MNP to 20.3 ~33.2 mV for chitosan-MNP, depending on the amount of chitosan used in the reaction (Table 1). Moreover, the change in zeta potential correlates well with the change in surface density of $-NH_2$ groups, which increases from 119.5 to 1962 μmole/mg particle (Table 1). The abundance of free amino groups hanging from the chitosan polymer chains in the composite particles facilitates the immobilization of tPA by glutaraldehyde-mediated amide bond formation.

Fig. 3a shows the XRD patters of Fe_3O_4 MNP and chitosan-MNP. All particles have six characteristic peaks at $2\theta = 30.1^\circ$, 35.4°, 43.1°, 53.2°, 56.9°, and 62.5°, which can be indexed to the (2 2 0), (3 1 1), (4 0 0), (4 2 2), (5 1 1), and (4 4 0) planes of a cubic cell. The crystalline structure of the particle can be confirmed to correspond to that of magnetite structure (JCPDS card number 19-0629) and reveal that all resultant nanoparticles were pure Fe_3O_4 with a spinel structure. It is also evident that the chitosan coating process did not result in a phase change of Fe_3O_4 MNP. The average crystal grain sizes are from 9.3 to 10.0 nm (Table 1), calculated from the Scherrer equation with XRD line broadening assuming crystals are spherical,

$$\tau = \frac{0.9\lambda}{\beta \cos\theta} \quad (1)$$

where τ is the mean size of the ordered (crystalline) domains, λ is the wavelength of the X-ray (1.54056 Å), θ is the diffraction angle in degree, and β in radian is the measured full width at half maximum intensity. The diffraction peak at $2\theta = 35.4^\circ$, which corresponds to the lattice plane (3 1 1), was used for calculation because this peak is well resolved and shows no interferences.

FT-IR analysis was performed to confirm the synthesis of chitosan-MNP. For chitosan-MNP, the presence of Fe_3O_4 MNP could be confirmed by the strong absorption peak corresponding to the Fe–O bond at 580 cm^{-1} and all absorption peaks corresponding to chitosan at 1084, 1322, 1381, 1428, 1656, 2904, and 3450 cm^{-1} (data not shown).

The magnetic properties of Fe_3O_4 MNP and chitosan-MNP are shown in Fig. 3b. From the magnetization curve, the remanence (residue magnetization) and coercive force (the applied field that reduces magnetization to zero) were zero and there was no magnetic hysteresis loop observed, indicating the characteristic superparamagnetic behavior of MNP. This is expected for magnetic materials with size less than 10 nm (Mikhaylova et al., 2004). This result also indicates that only single domain MNP is present in chitosan-MNP. Superparamagnetism (i.e. responsiveness to an applied magnetic field without retaining any magnetism after removal of the magnetic field) is an especially important property needed for magnetic targeted carriers. The saturated magnetizations are 68.3, 52.3, 43.4, 26.4, 23.2, and 14.5 emu/g for MNP, C125, C250, C500, C1000, and C2000, respectively. Particle size difference is ruled out as the main reason for decrease in saturation magnetization since the difference is only less than 10% from XRD calculations. Because the weights of all particles used for the measurement of magnetic properties were constant, decreasing saturation magnetization is expected for chitosan-MNP with increasing chitosan weight percentage. Nonetheless, the saturation magnetization would also decrease when Fe_3O_4 MNP is covered by polymer molecules. Chitosan-MNP coated with more chitosan apparently will therefore lead to a lower saturation magnetization (Nara, Torii, & Tasumi, 1996). Even though the saturation magnetization value of Fe_3O_4 MNP decreases after chitosan coating, it is higher than that when Fe_3O_4 MNP was modified with oleic

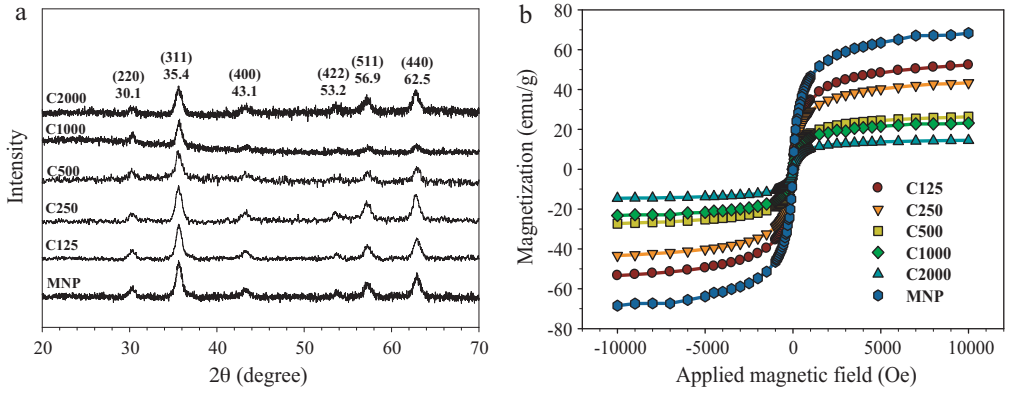

Fig. 3. (a) X-ray diffraction patterns, and (b) superconducting quantum interference device magnetization curves of Fe_3O_4 magnetic nanoparticle (MNP) and chitosan-coated magnetic nanoparticle (C125–C2000).

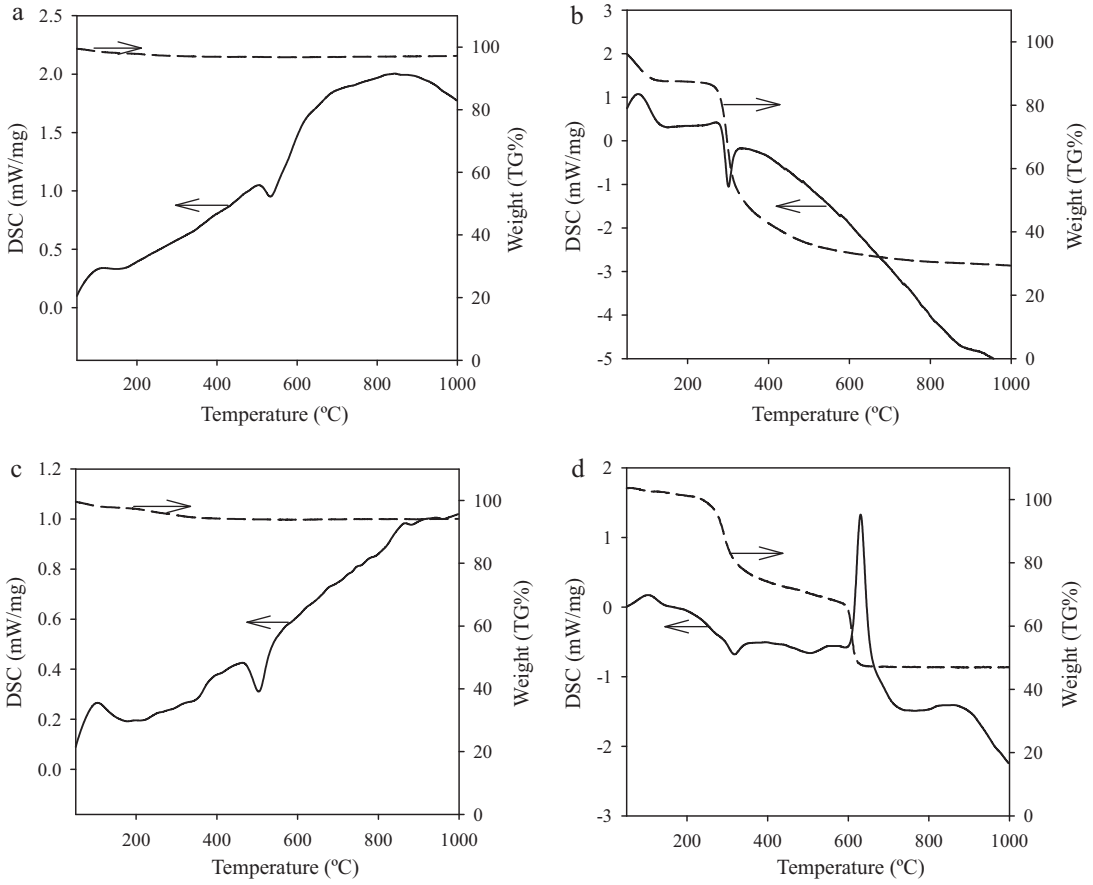

Fig. 4. Thermogravimetric and differential thermal analysis curves of (a) Fe_3O_4 magnetic nanoparticle (MNP); (b) chitosan; (c) chitosan-coated magnetic nanoparticle (C250); (d) chitosan-coated magnetic nanoparticle (C1000).

acid or encapsulated within a polymer matrix (Tanyolac & Ozdural, 2000).

Thermogravimetric and differential thermal analysis results are shown in Fig. 4. For chitosan powder, complete thermal decomposition occurred at around 600 °C. However, for C500, C1000, and C2000, chitosan coated on the particle surface complete decomposed only when the temperature increased above 700 °C. From 200 to 400 °C, there was no weight loss in Fe_3O_4 MNP but chitosan experienced a 47.1% weight loss due to the decomposition of polysaccharide units. Within the interval of 600–650 °C, the weight loss percentages of chitosan, Fe_3O_4 MNP, and C250 were negligible without any change of heat flow. In contrast, the weight-loss percentages of C500, C1000, and C2000 were 12.6%, 17.7% and 19.9%, respectively, with a significant endothermic peak. Taken together, this indicates the interactions between Fe_3O_4 MNP and chitosan is stronger in C500, C1000, and C2000 than in C125 or C250, which also raised the decomposition temperature of the coated chitosan. The weight percentage of chitosan in chitosan-MNP can be calculated according to the following formula (Peniche, Osorio, Acosta, de la Campa, & Peniche, 2005),

$$\frac{R_q}{\Delta W_c} \times \Delta W_m + M = R \tag{2}$$

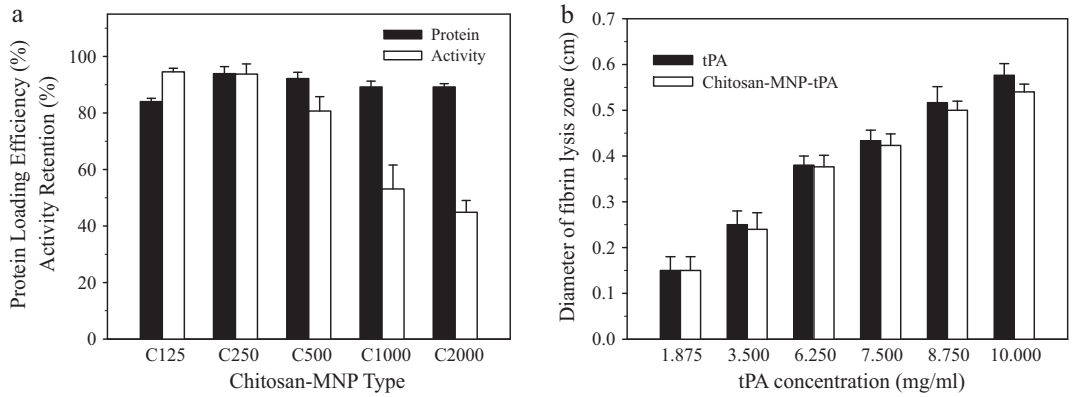

Fig. 5. (a) Protein loading efficiency and activity retention of tPA immobilized to different chitosan-coated magnetic nanoparticles (C125–C2000). (b) Fibrinolytic activities of tPA and tPA bound to chitosan-coated magnetic nanoparticle (C250) by fibrin clot lysis assay.

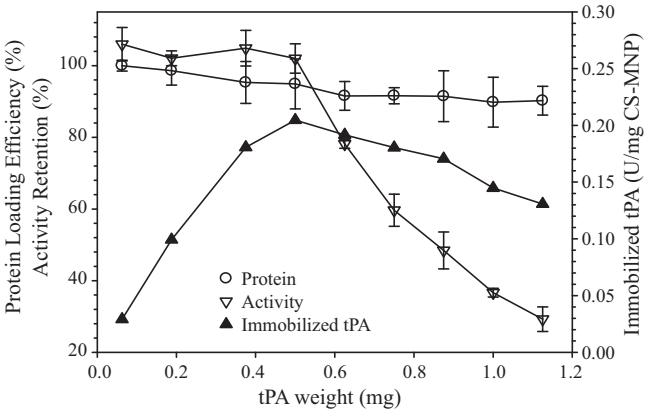

Fig. 6. The effects of the amount of tPA added during immobilization on the protein loading efficiency and activity retention of tPA immobilized to chitosan-coated magnetic nanoparticle (5 mg C250).

where R_q is the residue (wt%) at 1000 °C of chitosan, ΔW_c and ΔW_m are the weight-loss percentages for chitosan and chitosan-MNP within the interval of 200–400 °C, respectively, M is the weight percentage of chitosan in chitosan-MNP, and R is the residue (wt%) at 1000 °C for chitosan-MNP.

The weight percentages of chitosan in chitosan-MNP calculated from Eq. (2) are included in Table 1. The results indicated that the fraction of chitosan in chitosan-MNP increased with the concentration of chitosan used in the synthesis, which is consistent with an expected increase of chitosan coating thickness on chitosan-MNP surface. Iron oxide (Fe_3O_4) content determined separately by inductively coupled plasma optical emission spectroscopy also confirmed the trend observed (Table 1). However, the increase of chitosan in chitosan-MNP does not lead to a concomitant increase of surface –NH_2 groups (Table 1), indicating some coated chitosan molecules are not exposed on the surface. It is also interesting to note that higher chitosan content in the nanoparticle does not lead to an increase of hydrodynamic diameter of chitosan-MNP measured by dynamic light scattering (Table 1).

The cytotoxicity of chitosan-MNP in suspension was examined using the MTT method. The MTT assay is a simple nonradioactive colorimetric assay to measure the level of cell viability. MTT is a yellow, water-soluble, tetrazolium salt. Metabolically active cells can convert this dye into a water-insoluble dark blue formazan by the reductive cleavage of the tetrazolium ring (Mosmann, 1993). Formazan crystals can then be dissolved in an organic solvent and quantified by measuring the absorbance of the solution, which is related to the number of living cells. The relative 3T3 cell survival when exposed to chitosan-MNP was >96% when 3T3 cells without contacting chitosan-MNP were used as the control (data not shown). There is also no statistical difference from the control for all samples ($p < 0.05$). Since the threshold cytotoxic concentration of magnetic nanoparticles has been reported to be within our testing range (Gupta & Gupta, 2005), the in vitro biocompatibility test indicated that chitosan-MNP elicited no cytotoxicity.

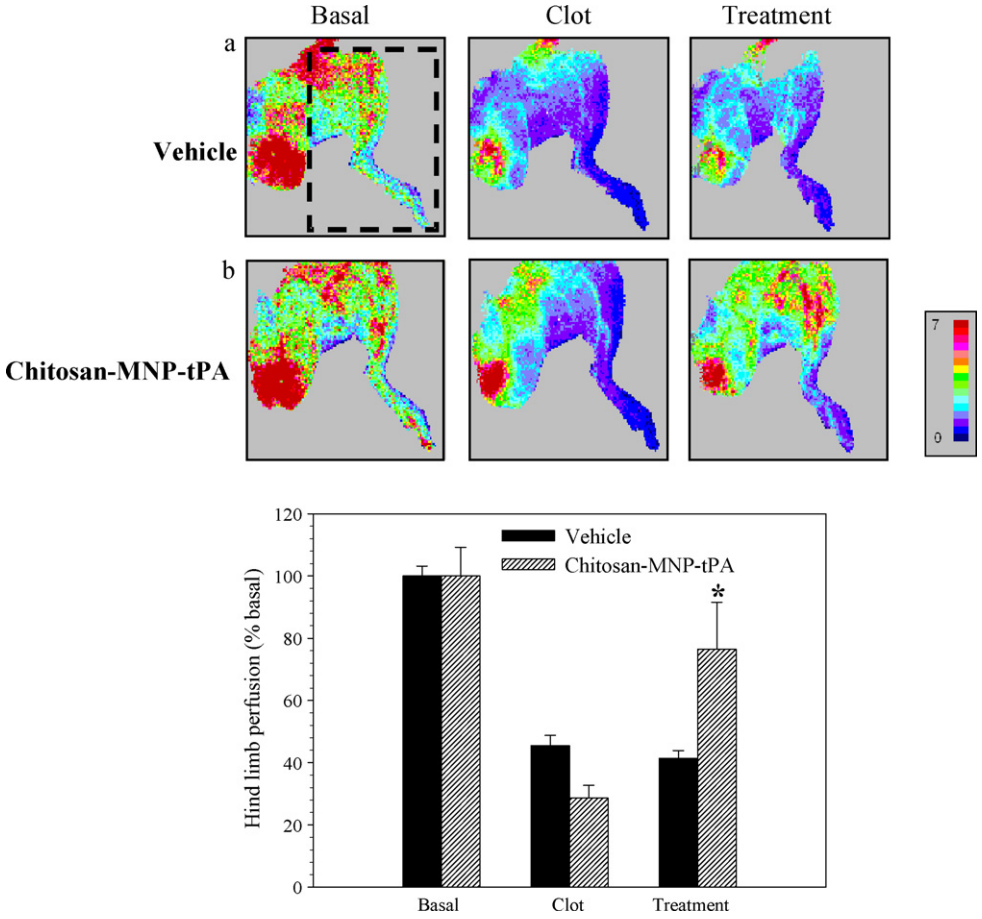

Fig. 7. Representative results of the effects of tPA immobilized to chitosan-coated magnetic nanoparticle (chitosan-MNP–tPA) on tissue perfusion in a rat iliac embolic model. Tissue perfusion of hind limb was measured with a laser Doppler perfusion imager. Five minutes after clot lodging, vehicle (a) or tPA covalently bound to chitosan-coated magnetic particle C250 (b) was administered from the right iliac artery under magnet guidance and treated for 120 min. Laser Doppler signals in designated areas, as illustrated with the square in (a), were acquired for quantitative analysis of hind limb perfusion. *$p < 0.05$ compared with vehicle.

3.2. Preparation and properties of tPA immobilized to chitosan-coated magnetic nanoparticle

The protein loading efficiency calculated from the amount of tPA covalently immobilized to chitosan-MNP is >80% for all preparations (Fig. 5a). One of the major challenges of enzyme immobilization to MNP is loss of enzyme activity after immobilization (Koneracka et al., 1999). Covalent immobilization of tPA to chitosan-MNP by glutaraldehyde may potentially involve amino acids of tPA necessary for substrate recognition or catalytic activity, which will result in loss of the enzyme activity after immobilization. To determine whether the bound tPA retained its enzyme activity, the chromogenic substrate assay was first conducted for comparison of the specific activity of free and immobilized tPA. As can be seen from Fig. 5a, the activity retention is higher (~100%) for chitosan-MNP prepared with less chitosan (C125 and C250). Reduced activity retention for chitosan-MNP prepared at higher chitosan concentrations, which contain more surface $-NH_2$ groups (Table 1), may be due to increased crosslinking between chitosan-MNP and tPA. Excessive crosslinking could distort native enzyme structure and lead to reduced tPA specific activity. Considering saturation magnetization, protein loading efficiency, and activity retention, C250 was deemed as the best preparation and will be used in the following studies.

From fibrin clot lysis assay, the fibrinolytic activity of chitosan-MNP–tPA is not different from free tPA ($p < 0.05$) for concentrations up to 10 mg/ml tPA, suggesting that all fibrinolytic enzyme activity of tPA could be preserved after covalent immobilization to chitosan-MNP (Fig. 5b). Covalent binding of tPA to C250 hence preserved most of its fibrinolytic activity, which is critical for effective thrombolysis in vivo. After chitosan coating, the resulting chitosan-MNP possesses excellent colloidal stability in solution, which not only withstands repeated centrifugation/re-dispersion cycles without aggregation, but also exerts a characteristic required for effective interaction with the fibrin clot in vivo.

The effect of the concentration of tPA used for immobilization was studied and the results are shown in Fig. 6. The protein loading efficiency and the activity retention are higher than 90% up to 0.5 mg tPA, which subsequently decrease at higher tPA loadings. The immobilized tPA activity per mg of chitosan-MNP–tPA will be important in order to inject the least amount of nanoparticles during in vivo application. This value also reached a plateau at around 0.5 mg tPA. The optimum drug loading is therefore reached when 0.5 mg tPA is reacted with 5 mg chitosan-MNP, where 95% drug is attached to the magnetic carrier with full retention of its activity.

3.3. Ex vivo thrombolysis model and in vivo rat embolic model

Using the ex vivo intravascular thrombolysis model in Fig. 1, we studied the efficacy of thrombolysis by chitosan-MNP–tPA under magnetic targeting. The blood clot lysis time, which is determined from the time to blood flow from capillary, is shown at the bottom of Fig. 1. No clot lysis was observed for controls using PBS or chitosan-MNP (with or without magnet). Chitosan-MNP–tPA under magnetic guidance can reduce the blood clot lysis time by 58% compared to runs without magnetic targeting or by 53% compared to free tPA using the same dosage of the thrombolytic drug (0.1 mg tPA/ml). Magnetic targeted delivery of chitosan-MNP–tPA, a new form of thrombolytic drug potentially useful for the treatment of thrombus, can therefore effectively shorten the thrombolysis time compared with the conventional treatment with free tPA under the same drug dosage. By reducing the dosage of tPA for treatment by delivering the drug bound to chitosan-MNP and under magnetic guidance, the hemorrhagic side effect can be prevented.

From the results of rat embolic model, introducing a whole blood clot to the left iliac artery dramatically attenuated the hind limb perfusion after equilibration (Fig. 7). Administration of a dosage of chitosan-MNP–tPA with activity equivalent to 0.2 mg/kg of free tPA plus magnetic guidance significantly increased tissue perfusion from $29 \pm 4\%$ to $77 \pm 15\%$ of the basal levels before clot introduction ($n = 3$; $p < 0.05$ by paired Student's t-test). Whereas vehicle administration did not improve the hind limb perfusion in the control group ($n = 8$). As restriction in blood supply caused by introduced blood clot will lead to damages of blood vessels, subsequent reperfusion of blood after tPA-induced thrombolysis may therefore prevent a full recovery of the hemodynamics (Garden & Granger, 2000). Nonetheless, the recovery of 70–80% blood flow with magnetically guided chitosan-MNP–tPA at a dosage of 0.2 mg/kg tPA represents 20% the dose (1 mg/kg) required for thrombolysis by free tPA (Ma et al., 2007).

4. Conclusion

Chitosan-MNP with different chitosan contents could be prepared and used for covalent immobilization of tPA with a high protein loading efficiency and retention of activity. The optimum drug loading is reached when 0.5 mg tPA is reacted with 5 mg C250, where all tPA is immobilized to the carrier with full retention of its thrombolytic activity. Chitosan-MNP–tPA under magnetic guidance requires only one-fifth of the regular dose of tPA to exert a similar thrombolytic efficacy of the drug. Biocompatible chitosan-MNP–tPA developed in this study will be useful as a magnetic targeted drug to improve clinical thrombolytic therapy.

Acknowledgements

Financial supports from the National Science Council (98-2120-M-182-001), the National Health Research Institute (NHRI-EX99-9937EI), and the Chang Gung Memorial Hospital (CMRPD250023) are highly appreciated.

References

Anderson, H. V., & Willerson, J. T. (1993). Thrombolysis in acute myocardial infarction. *New England Journal of Medicine*, *329*, 703–709.

Berny, M. A., Patel, I. A., White-Adams, T. C., Simonson, P., Gruber, A., Rugonyi, S., et al. (2010). Rational design of an ex vivo model of thrombosis. *Cellular and Molecular Bioengineering*, *3*, 187–189.

Berry, C. C., & Curtis, A. S. G. (2003). Functionalisation of magnetic nanoparticles for applications in biomedicine. *Journal of Physics: Applied Physics*, *36*, R198–R206.

Chung, T. W., Wang, S. S., & Tsai, W. J. (2008). Accelerating thrombolysis with chitosan-coated plasminogen activators encapsulated in poly-(lactide-co-glycolide) (PLGA) nanoparticles. *Biomaterials*, *29*, 228–237.

Dang, J. M., & Leong, K. W. (2006). Natural polymers for gene delivery and tissue engineering. *Advanced Drug Delivery Reviews*, *58*, 487–499.

Denkbas, E. B., & Ottenbrite, R. M. (2006). Perspectives on chitosan drug delivery systems: Based on their geometries. *Journal of Bioactive and Compatible Polymers*, *21*, 351–368.

Dobson, J. (2006). Magnetic nanoparticles for drug delivery. *Drug Development Research*, *67*, 55–60.

Donadel, K., Felisberto, M. D. V., Fávere, V. T., Rigoni, M., Batistela, N. J., & Laranjeira, M. C. M. (2008). Synthesis and characterization of the iron oxide magnetic particles coated with chitosan biopolymer. *Materials Science and Engineering C*, *28*, 509–514.

Fang, C., & Zhang, M. (2009). Multifunctional magnetic nanoparticles for medical imaging applications. *Journal of Materials Chemistry*, *19*, 6258–6266.

Garden, C. L., & Granger, D. N. (2000). Pathophysiology of ischemia–reperfusion injury. *Journal of Pathology*, *190*, 255–266.

Gaur, U., Sahoo, S. K., De, T. K., Ghosh, P. C., Maitra, A., & Ghosh, P. K. (2000). Biodistribution of fluoresceinated dextran using novel nanoparticles evading reticuloendothelial system. *International Journal of Pharmaceutics*, *202*, 1–10.

Gupta, A. K., & Gupta, M. (2005). Synthesis and surface engineering of iron oxide nanoparticles for biomedical applications. *Biomaterials*, *26*, 3995–4021.

Huang, H. Y., Shieh, Y. T., Shih, C. M., & Twu, Y. K. (2010). Magnetic chitosan/iron (II, III) oxide nanoparticles prepared by spray-drying. *Carbohydrate Polymers*, *81*, 906–910.

Huber, K., Runge, M. S., Bode, C., & Gulba, D. (1996). Thrombolytic therapy in acute myocardial infarction. *Annals of Hematology*, *73*, S29–S38.

Janes, K. A., Calvo, P., & Alonso, M. J. (2001). Polysaccharide colloidal particles as delivery systems for macromolecules. *Advanced Drug Delivery Reviews*, *47*, 83–97.
Janolino, V. J., & Swaisgood, H. E. (1992). A spectrophotometric assay for solid phase primary amino groups. *Applied Biochemistry and Biotechnology*, *36*, 81–85.
Kaminski, M. D., Xie, Y., Mertz, C. J., Finck, M. R., Chen, H., & Rosengart, A. J. (2008). Encapsulation and release of plasminogen activator from biodegradable magnetic microcarriers. *European Journal of Pharmaceutical Sciences*, *35*, 96–103.
Katas, H., & Alpar, H. O. (2006). Development and characterisation of chitosan nanoparticles for siRNA delivery. *Journal of Controlled Release*, *115*, 216–225.
Kim, E. H., Lee, H. S., Kwak, B. K., & Kim, B. K. (2005). Synthesis of ferrofluid with magnetic nanoparticles by sonochemical method for MRI contrast agent. *Journal of Magnetism and Magnetic Materials*, *289*, 328–330.
Koneracka, M., Kopcansky, P., Antalik, M., Timko, M., Ramchand, C. N., & Lobo, D. (1999). Immobilization of proteins and enzymes to fine magnetic particles. *Journal of Magnetism and Magnetic Materials*, *201*, 427–430.
Kumar, M., Muzzarelli, R. A. A., Muzzarelli, C., Sashiwa, H., & Domb, A. J. (2004). Chitosan chemistry and pharmaceutical perspectives. *Chemical Reviews*, *104*, 6017–6084.
Li, G. Y., Jiang, Y. R., Huang, K. L., Ding, P., & Chen, J. (2008). Preparation and properties of magnetic Fe_3O_4–chitosan nanoparticles. *Journal of Alloys and Compounds*, *466*, 451–456.
Liang, J. F., Song, H., Li, Y. T., & Yang, V. C. (2000). A novel heparin/protamine-based pro-drug type delivery system for protease drugs. *Journal of Pharmaceutical Sciences*, *89*, 664–673.
Ma, Y. H., Hsu, Y. W., Chang, Y. J., Hua, M. Y., Chen, J. P., & Wu, T. (2007). Intra-arterial application of magnetic nanoparticle for targeted thrombolytic therapy: A rat embolic model. *Journal of Magnetism and Magnetic Materials*, *311*, 342–346.
Ma, Y. H., Wu, S. Y., Wu, T., Chang, Y. J., Hua, M. Y., & Chen, J. P. (2009). Magnetically targeted thrombolysis with recombinant tissue plasminogen activator bound to polyacrylic acid. *Biomaterials*, *30*, 3343–3351.
Majeti, N. V., & Kumar, R. (2000). A review of chitin and chitosan applications. *Reactive and Functional Polymers*, *46*, 1–27.
Mikhaylova, M., Kim, D. K., Bobrysheva, N., Osmolowsky, M., Semenov, V., Tsakalakos, T., et al. (2004). Superparamagnetism of magnetite nanoparticles: Dependence on surface modification. *Langmuir*, *20*, 2472–2477.
Mosmann, T. (1993). Rapid colorimetric assay for cellular growth and survival: Application to proliferation and cytotoxic assay. *Journal of Immunological Methods*, *95*, 55–63.
Nara, M., Torii, H., & Tasumi, M. (1996). Correlation between the vibrational frequencies of the carboxylate group and the types of its coordination to a metal ion: An ab initio molecular orbital study. *Journal of Physical Chemistry*, *100*, 19812–19817.
Peniche, H., Osorio, A., Acosta, N., de la Campa, A., & Peniche, C. (2005). Preparation and characterization of superparamagnetic chitosan microspheres: Application as a support for the immobilization of tyrosinase. *Journal of Applied Polymer Science*, *98*, 651–657.
Smith, B. J. (1999). Thrombolysis in acute myocardial infarction: Analysis of studies comparing accelerated t-PA and streptokinase. *Journal of Accident and Emergency Medicine*, *16*, 407–411.
Sood, A. K., Mangala, L. S., Han, H., Lu, C., Ali-Fehmi, R., Stone, R., et al. (2009). In vivo angiogenic gene silencing using chitosan nanoparticles in ovarian carcinoma. *Gynecologic Oncology*, *112*, 136–137.
Sun, C., Lee, J. S. H., & Zhang, M. (2008). Magnetic nanoparticles in MR imaging and drug delivery. *Advanced Drug Delivery Review*, *60*, 1252–1265.
Tanyolac, D., & Ozdural, A. R. (2000). A new low cost magnetic material: Magnetic polyvinylbutyral microbeads. *Reactive and Functional Polymers*, *43*, 279–286.
Tartaj, P., Morales, M., Gonzalez-Carreno, T., Veintemillas-Verdaguer, S., & Serna, C. (2005). *Journal of Magnetism and Magnetic Materials*, *290–291*, 28–34.
Wu, T., Hua, M. Y., Chen, J. P., Wei, K. C., Jung, S. M., Chang, Y. J., et al. (2007). Effects of external magnetic field on biodistribution of nanoparticles: A histological study. *Journal of Magnetism and Magnetic Materials*, *311*, 372–375.
Xie, Y., Kaminski, M. D., Torno, M. D., Finck, M. R., Liu, X., & Rosengart, A. J. (2007). Physicochemical characteristics of magnetic microspheres containing tissue plasminogen activator. *Journal of Magnetism and Magnetic Materials*, *311*, 376–378.